

Topological schemes for the electrodynamic Aharonov-Bohm effect

Pablo L. Saldanha^{1,*} and Herman Batelaan²

¹*Departamento de Física, Universidade Federal de Minas Gerais, Belo Horizonte, MG 31270-901, Brazil*

²*Department of Physics and Astronomy, University of Nebraska—Lincoln,*

208 Jorgensen Hall, Lincoln, Nebraska 68588-0299, USA

(Dated: November 15, 2024)

We consider different schemes for the electrodynamic Aharonov-Bohm (AB) effect introduced in Ref. [Phys. Rev. A **108**, 062218 (2023)], exploring subtleties of the phenomenon to enhance the understanding of its topological nature. In the treated examples, the electric current in a solenoid varies in time, changing its internal magnetic field and producing an external electric field, while a quantum charged particle is in a superposition state inside two Faraday cages in an interferometer. The Faraday cages cancel the electric field at their interiors, such that the particle is always subjected to null electromagnetic fields. We discuss how the AB phase difference depends on the topology of the electric and magnetic fields in spacetime in the different treated situations.

The Aharonov-Bohm (AB) effect [1, 2] is a striking quantum phenomenon that contradicts the idea that electric charges are affected only by the local electromagnetic fields. In the magnetic AB effect [1, 2], the interference pattern of quantum charged particles in an interferometer, whose possible paths enclose a long solenoid, depends on the solenoid's magnetic flux even if the particles only propagate in regions with negligible electromagnetic fields. In the electric AB effect [2], the interference pattern of quantum charged particles depends on the electric potentials applied to the different interferometer paths during the particles passage even if the particles are always subjected to negligible electromagnetic fields. Several experiments performed with different systems have confirmed the AB effect [3–14].

The magnetic AB effect is frequently described as a topological effect [15–19]. A topological description of the electric AB effect was recently given [20], by considering the topologies of the electromagnetic field configuration and possible particles trajectories in spacetime. This description permitted the prediction of a novel electrodynamic AB effect, where a nonzero AB phase difference appears in a situation where the magnetic flux in a solenoid varies while the quantum particle is in a superposition state inside two Faraday cages in an interferometer, even if the particle paths enclose no magnetic flux and are subjected to a negligible scalar potential difference [20]. Here we present and explore subtleties of the electrodynamic AB effect introduced in Ref. [20] in novel situations, providing a deeper understanding of the AB effect, regarding its topological nature.

Consider the situation depicted in Fig. 1(a), with a Mach-Zehnder interferometer for a non-relativistic quantum charged particle. The initial magnetic flux in the infinite solenoid is Φ_i . While the quantum particle is in a superposition state inside both Faraday cages, which are symmetrically positioned in relation to the solenoid as shown in the figure, its electric current varies, with the

final magnetic flux being Φ_f . This change of the electric current produces an electric field in the interferometer, but the Faraday cages cancel the fields at their interior, such that the quantum particle is subjected to null electromagnetic fields. The quantum particle then continues its evolution through the interferometer, always in regions with null electromagnetic fields.

In Ref. [20], following Ref. [21], it was discussed how the AB phase difference between the interferometer paths in any AB scheme can be written as

$$\phi_{AB} = \frac{q}{\hbar} \left[\int_S d\mathbf{a}(t) \cdot \mathbf{B}(\mathbf{r}, t) - \int \int_S dt d\mathbf{r}(t) \cdot \mathbf{E}(\mathbf{r}, t) \right], \quad (1)$$

where q is the particle charge, \mathbf{E} is the electric field, \mathbf{B} is the magnetic field, and S is a spacetime surface bounded by the worldlines of the two interfering paths. This surface can be constructed from the deformation of one of the particle possible trajectories in the interferometer in spacetime into the other, in the following way. Consider that at each time instant t , the quantum particle is in a superposition state with wavepackets centered at two positions $\mathbf{x}_a(t)$ (in path a) and $\mathbf{x}_b(t)$ (in path b). Draw an arbitrary curve that goes from $\mathbf{x}_a(t)$ to $\mathbf{x}_b(t)$ for each time instant t , through infinitesimal displacements $d\mathbf{r}(t)$. The spatial component $d\mathbf{a}(t)$ of the surface between times t and $t + dt$ is obtained by the minimum area whose contour are the curves that connect $\mathbf{x}_a(t)$ and $\mathbf{x}_a(t + dt)$, $\mathbf{x}_a(t + dt)$ and $\mathbf{x}_b(t + dt)$, $\mathbf{x}_b(t + dt)$ and $\mathbf{x}_b(t)$, and $\mathbf{x}_b(t)$ and $\mathbf{x}_a(t)$. More details can be found in Ref. [20]. An example of such deformation is the blue surface in Fig. 1(b). The two possible particle trajectories in spacetime are represented in black. The initial magnetic field is represented in yellow, while the final one is in orange. The spacetime region with a nonzero electric field is represented in green. It can be seen that the region with null electromagnetic fields is not simply connected in spacetime. It is not possible to deform one of the possible particle trajectories in spacetime into the other, keeping the initial and final points fixed, without crossing a region with nonzero electromagnetic fields. The AB phase difference of Eq. (1) depends on the topologies of

* saldanha@fisica.ufmg.br

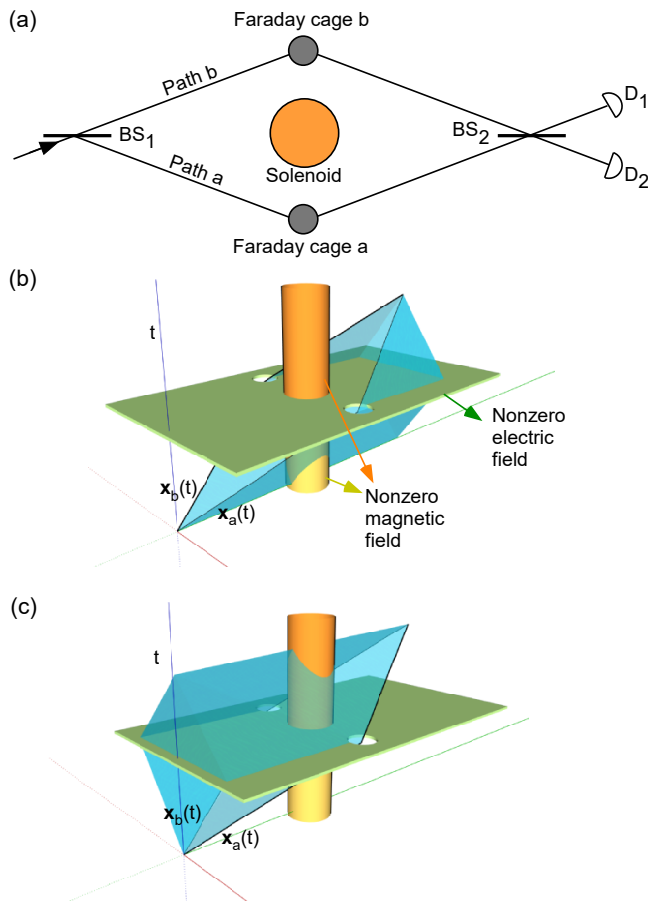


FIG. 1. (a) Scheme of an electrodynamic AB interferometer for a quantum charged particle. BS_1 and BS_2 are beam splitters, D_1 and D_2 are detectors. The particle is sent to the interferometer as indicated by the arrow. While the quantum particle is in a superposition state inside both Faraday cages, the solenoid current is changed. (b) The possible spacetime trajectories $\mathbf{x}_a(t)$ and $\mathbf{x}_b(t)$ of the quantum particle in the interferometer are represented in black. The time coordinate is in the vertical direction and the trajectories are in the xy plane. The spacetime regions with nonzero magnetic field are represented in orange and yellow, with these two colors representing two different values for the field. The spacetime region with nonzero electric field is represented in green. The spacetime surface formed by one possible deformation of the spacetime trajectory $\mathbf{x}_a(t)$ into the spacetime trajectory $\mathbf{x}_b(t)$ is represented in blue. (c) The same as in (b), but with a different spacetime surface in blue formed by a different deformation of the spacetime trajectory $\mathbf{x}_a(t)$ into the spacetime trajectory $\mathbf{x}_b(t)$.

the electromagnetic fields and possible particle trajectories in spacetime, not on specific geometric configurations [20]. Note, that we will consider schemes for which the interferometer lengths are small and the timescales are large, such that the fields propagation times within the interferometer can be disregarded.

Now let us compute the AB phase difference between the paths in the scheme of Fig. 1(a) using Eq. (1) with

the spacetime surface represented in Fig. 1(b). Note that the initial magnetic flux crosses the spacetime surface of Fig. 1(b), such that the contribution of the first term on the right side of Eq. (1) to the AB phase difference is $q\Phi_i/\hbar$. In the Lorenz gauge, a long cylindrical solenoid with a magnetic flux Φ produces a vector potential $\mathbf{A} = \Phi/(2\pi\rho)\hat{\phi}$ outside it, in cylindrical coordinates (ρ, ϕ, z) . While the solenoid current varies, it generates an electric field $\mathbf{E}_A = -\partial\mathbf{A}/\partial t$ in the $\hat{\phi}$ direction. Charge densities are induced in the Faraday cages, creating an electric field \mathbf{E}_V that cancels the total electric field at their interior. We consider that the center of the Faraday cages are in positions \mathbf{R}_j , with $j = \{a, b\}$. The total electric field can be written as $\mathbf{E} = \mathbf{E}_A + \mathbf{E}_V$, which enters in the second term on the right side of Eq. (1).

Due to the system symmetry, the induced charges are symmetric with a rotation of 180 degrees around the solenoid axis, such that the electric field \mathbf{E}_V produced by these induced charges is also symmetric with this rotation. Any closed loop integral at constant t , $\oint d\mathbf{r} \cdot \mathbf{E}_V(\mathbf{r})$, for the field \mathbf{E}_V , due to the induced charge distribution, equals zero. Combined with rotational symmetry of \mathbf{E}_V , the line integral $\int_{\mathbf{R}_a}^{\mathbf{R}_b} \mathbf{E}_V \cdot d\mathbf{r} = 0$ over the line defined by the intersection of the green and blue surface at any time during which the electron is in the Faraday cage in Fig. 1(b) equals zero. So, \mathbf{E}_V does not contribute to the AB phase of Eq. (1) in this case.

But we do have a contribution of the field $\mathbf{E}_A = -\partial\mathbf{A}/\partial t$ to the AB phase of Eq. (1). Calling t_0 the time when the current in the solenoid starts to vary and t_1 the time when it becomes stationary again, the contribution of the second term on the right side of Eq. (1) to the AB phase difference is

$$\frac{q}{\hbar} \int_{t_0}^{t_1} dt \int_{\mathbf{R}_a}^{\mathbf{R}_b} d\mathbf{r} \cdot \frac{\partial\mathbf{A}}{\partial t} = \frac{q}{\hbar} \left[\int_{\mathbf{R}_a}^{\mathbf{R}_b} d\mathbf{r} \cdot \mathbf{A} \right]_{t_0}^{t_1} = \frac{q}{2\hbar} (\Phi_f - \Phi_i), \quad (2)$$

considering a negligible size for the Faraday cages. To arrive at the above result, each path integral was divided into infinitesimal dislocations in the directions $\hat{\rho}$ and $\hat{\phi}$, such that only the dislocations in the direction $\hat{\phi}$ contribute for the integral. If the Faraday cages are not so small, there would be a correction by a numerical factor of the order of $\Delta\theta/\pi$ in the above result, where $\Delta\theta$ is the angle formed by the lines that go from the solenoid center to each of the extremities of one of the cages in Fig. 1(a).

So, we conclude that the total AB phase difference between the paths in the scheme of Fig. 1(a) is $q(\Phi_i + \Phi_f)/(2\hbar)$. This result makes sense, since the total AB phase difference depends on the average magnetic flux enclosed by the paths during the particle propagation through the interferometer.

If we consider the spacetime surface of Fig. 1(c), the contribution of the first term on the right side of Eq. (1) is $q\Phi_f/\hbar$ and the contribution of the second term is $q(\Phi_i - \Phi_f)/(2\hbar)$, resulting in the same total AB phase dif-

ference. The sign of the latter contribution has changed as the direction of the path integration starting at \mathbf{R}_a and ending at \mathbf{R}_b has changed in Eq. (2), being clockwise instead of counterclockwise. Note that in the scheme of Fig. 1(a) both terms of Eq. (1) contribute for the total AB phase difference, no matter what spacetime surface is constructed, as long as Φ_i and Φ_f have different values, both different from zero. This wasn't true in the examples treated in Ref. [20], where the particle paths did not enclose the solenoid. In the examples treated there, for specific spacetime surfaces one of the two terms on the right side of Eq. (1) could have a null contribution for the AB phase. This is an important novelty of the AB scheme of Fig. 1(a) treated here. To our knowledge, it is the first AB scheme where both the electric and magnetic field configurations necessarily contribute for the total AB phase difference between the interferometer paths, being a truly *electromagnetic* AB effect.

Now let us consider the scheme of Fig. 2(a), similar to the one of Fig. 1(a). Again, the magnetic flux in the infinite solenoid varies from an initial value Φ_i to a final value Φ_f while the quantum particle is in a superposition state inside the Faraday cages. But now we have a metallic wire connecting the cages, as shown in the figure. Fig. 2(b) illustrates the two interferometric particle trajectories and the electromagnetic field configuration in spacetime. The total AB phase difference between the paths can be computed using Eq. (1) with the spacetime surface indicated in blue in Fig. 2(b). The contribution of the second term on the right side of Eq. (1) is zero for this spacetime surface, since there is no superposition of the blue surface with the green solid in this case (or, in other words, \mathbf{E} is zero over the surface of integration). The contribution of the first term is $q\Phi_i/\hbar$, which becomes the total AB phase difference. Interestingly, the AB phase difference does not depend on the final solenoid magnetic flux. The opposite happens in the scheme of Fig. 2(c), with the metallic wire turned to the other side of the solenoid. In an analogous way to Fig. 2(b), we can consider a spacetime surface with no superposition with the green solid, such that the second term on the right side of Eq. (1) does not contribute for the AB phase difference. However, in this case the first term results in $q\Phi_f/\hbar$. So, in this situation the AB phase difference is independent from the initial solenoid magnetic flux. This is an interesting subtlety of the effect: The AB phase difference depends on the position of the metallic wire that connects the Faraday cages.

To enhance the understanding of the above example, it can be compared to its description in a more conventional approach [2]. Consider the continuous accumulation of the AB phase difference acquired by the quantum particle during its propagation along its path through the interferometer, a view supported by works that use a quantum electromagnetic field to describe the interactions in the AB effect [22–26]. The AB phase results from the term $H_I = qV - (q/m)\mathbf{p} \cdot \mathbf{A}$ in the system Hamiltonian, where q , m , and \mathbf{p} are the particle charge, mass,

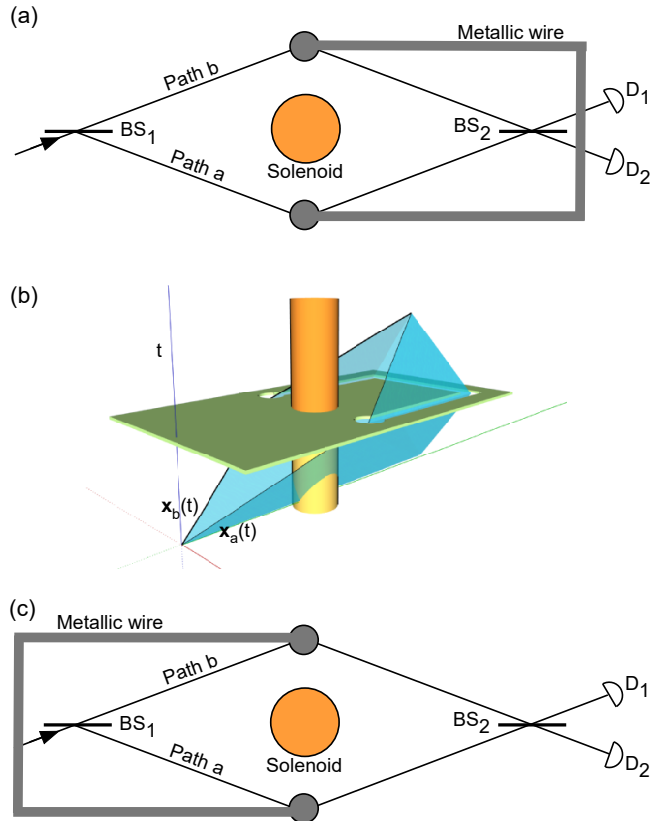


FIG. 2. (a) An interferometer similar to the one of Fig. 1(a), but now with a metallic wire connecting the two Faraday cages. Again, the solenoid current varies while the quantum particle is in a superposition state inside the Faraday cages. (b) Representation of the two interferometric particle trajectories and electromagnetic fields in spacetime, similarly to Fig. 1(b). Note that the spacetime surface (blue) formed by the deformation of one spacetime trajectory into the other has no superposition with the region with nonzero electric field (green) in this case. (c) The metallic wire of panel (a) is now turned to the other side of the solenoid.

and momentum respectively, and V and \mathbf{A} are the scalar and vector potentials. The AB phase accumulated in each path can be written as

$$\phi_i = - \int_{t_0}^t \frac{H_I}{\hbar} dt' = - \frac{q}{\hbar} \int_{t_0}^t V dt' + \frac{q}{\hbar} \int_{\mathbf{x}_0}^{\mathbf{x}_i} \mathbf{A} \cdot d\mathbf{x}, \quad (3)$$

where \mathbf{p}/m was substituted by the average wave packet velocity $d\mathbf{x}_i/dt$, we have $\mathbf{x}_a(t_0) = \mathbf{x}_b(t_0) = \mathbf{x}_0$ before the wave function splitting in the interferometer, and the spatial integral is performed through the particle path.

In the scheme of Fig. 2(a), while the particle propagates from BS₁ to the Faraday cages, the contribution for the AB phase difference can be computed by the second term on the right side of Eq. (3). In the Lorenz gauge, we have $\mathbf{A} = \Phi/(2\pi\rho)\hat{\phi}$ in cylindrical coordinates. Dividing the path integral into infinitesimal dislocations in the directions $\hat{\rho}$ and $\hat{\phi}$, we conclude that the contribution of the second term on the right side of Eq. (3) for

the AB phase difference is $q\Phi_i/(2\hbar)$ for very small cages. While the magnetic flux in the solenoid varies, an electric field $\mathbf{E}_A = -\partial\mathbf{A}/\partial t$ is created around it. Electric charges are then induced in the Faraday cages and in the metallic wire creating an electric field $\mathbf{E}_V = -\mathbf{E}_A$ inside them, canceling the total field. This generates a potential difference $V_a - V_b = -\int_{\mathbf{R}_b}^{\mathbf{R}_a} \mathbf{E}_V \cdot d\mathbf{r} = \int_{\mathbf{R}_b}^{\mathbf{R}_a} d\mathbf{r} \cdot \partial\mathbf{A}/\partial t$ between the Faraday cages. Using Eq. (2), we see that the first term on the right side of Eq. (3) results in a phase difference $q(\Phi_i - \Phi_f)/(2\hbar)$ during the variation of the solenoid magnetic flux. Finally, while the quantum particle propagates from the Faraday cages to BS₂, we have a contribution $q\Phi_f/(2\hbar)$ for the AB phase difference, that comes from the second term on the right side of Eq. (3). The three terms together results in a total AB phase difference $q\Phi_i/\hbar$, as previously deduced with the use of Eq. (1). Note that in the scheme of Fig. 2(c) the potential difference between the cages while the solenoid magnetic flux varies changes its sign, since the direction of \mathbf{E}_A (and consequently of \mathbf{E}_V) is inverted in opposite sides of the solenoid. This results in a total AB phase difference $q\Phi_f/\hbar$ in the scheme of Fig. 2(c), as previously computed.

We thus see that the AB phase difference between the paths in the schemes shown in Fig. 2 depends on the position of the metallic wire connecting the cages. This interesting behavior can be readily predicted with the spacetime diagrams as the one of Fig. 2(b). These examples show how these spacetime diagrams are useful for the prediction of novel interesting behaviors, besides evidencing the topological nature of the different kinds of AB effects.

Let us consider a last example, represented in Fig. 3, with the solenoid outside the interferometer, as in the situation considered in Ref. [20]. But now there is a metallic wire connecting the Faraday cages, giving N turns around the solenoid (with $N = 2$ in this figure). Again, the solenoid magnetic flux varies while the quantum particle is in a superposition state inside both Faraday cages. Electric charge densities are induced in the Faraday cages and in the metallic wire canceling the total electric field inside them. So, inside the wire the electric field generated by the induced charges is given by $\mathbf{E}_V = -\mathbf{E}_A = \partial\mathbf{A}/\partial t$. The potential difference between the Faraday cages can be written as

$V_a - V_b = -\int_{\mathbf{R}_b}^{\mathbf{R}_a} \mathbf{E}_V \cdot d\mathbf{r}$ in a path inside the metallic wire. Using this result in the first term of the right side of Eq. (3), we obtain a total AB phase difference $\pm Nq(\Phi_i - \Phi_f)/\hbar$, since the second term results in a null contribution in this configuration, and where the sign is determined by the winding direction consistent with the "half" winding of the example of Figure 2. We have an amplification effect on this electromagnetic AB phase difference given by the number of turns N of the metallic wire around the solenoid. In addition to illustrating a topological scheme, the amplification may be of use for the observation of the dispersionless nature of the Aharonov-Bohm effect for free electrons, which has re-

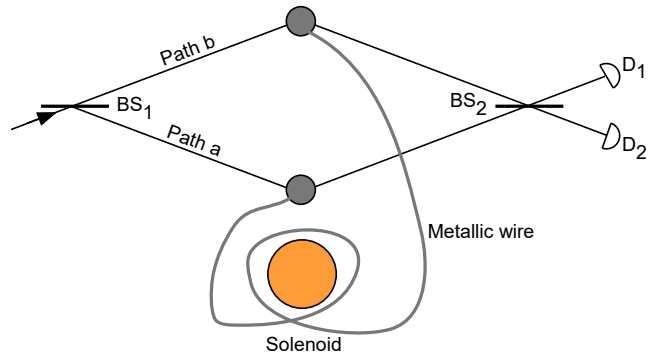


FIG. 3. Scheme of an electrodynamic AB interferometer for a quantum charged particle similar to the one of Fig. 1(a), but with the solenoid outside the interferometer. A metallic wire connects the two Faraday cages with $N = 2$ turns around the solenoid. Again, the solenoid current is changed while the quantum particle is in a superposition state inside both Faraday cages.

mained elusive [27].

To conclude, we have presented different physical schemes of the electrodynamic AB effect to illustrate what may be consider counter-intuitive behaviors associated with the AB effect and to reinforce its topological nature. The AB phase difference can always be computed by the general form of Eq. (1), depending on the topologies of the electromagnetic fields and of the particles trajectories in spacetime.

PLS was supported by the Brazilian agency CNPq (Conselho Nacional de Desenvolvimento Científico e Tecnológico). HB was supported by NSF award nr. 2207697.

-
- [1] W Ehrenberg and R E Siday, "The refractive index in electron optics and the principles of dynamics," Proc. Phys. Soc. B **62**, 8 (1949).
 [2] Y. Aharonov and D. Bohm, "Significance of electromagnetic potentials in the quantum theory," Phys. Rev. **115**, 485 (1959).
 [3] R. G. Chambers, "Shift of an electron interference pattern by enclosed magnetic flux," Phys. Rev. Lett. **5**, 3 (1960).

- [4] G. Matteucci and G. Pozzi, "New diffraction experiment on the electrostatic Aharonov-Bohm effect," Phys. Rev. Lett. **54**, 2469 (1985).
 [5] R. A. Webb, S. Washburn, C. P. Umbach, and R. B. Laibowitz, "Observation of $\frac{h}{e}$ Aharonov-Bohm oscillations in normal-metal rings," Phys. Rev. Lett. **54**, 2696 (1985).
 [6] A. Tonomura, N. Osakabe, T. Matsuda, T. Kawasaki, J. Endo, S. Yano, and H. Yamada, "Evidence for Aharonov-Bohm effect with magnetic field completely

- shielded from electron wave,” *Phys. Rev. Lett.* **56**, 792 (1986).
- [7] A. van Oudenaarden, M. H. Devoret, Y. V. Nazarov, and J. E. Mooij, “Magneto-electric Aharonov–Bohm effect in metal rings,” *Nature* **391**, 768 (1998).
- [8] A. Bachtold, C. Strunk, J.-P. Salvetat, J.-M. Bonard, L. Forró, T. Nussbaumer, and C. Schönberger, “Aharonov–Bohm oscillations in carbon nanotubes,” *Nature* **397**, 673 (1999).
- [9] Y. Ji, Y. Chung, D. Sprinzak, M. Heiblum, D. Mahalu, and H. Shtrikman, “An electronic Mach–Zehnder interferometer,” *Nature* **422**, 415 (2003).
- [10] H. Peng, K. Lai, D. Kong, S. Meister, Y. Chen, X.-L. Qi, S.-C. Zhang, Z.-X. Shen, and Y. Cui, “Aharonov–Bohm interference in topological insulator nanoribbons,” *Nat. Mater.* **9**, 225 (2010).
- [11] M. Becker, G. Guzzinati, A. Béch e, J. Verbeeck, and H. Batelaan, “Asymmetry and non-dispersivity in the Aharonov-Bohm effect,” *Nat. Commun.* **10**, 1700 (2019).
- [12] J. Nakamura, S. Fallahi, H. Sahasrabudhe, R. Rahman, S. Liang, G. C. Gardner, and M. J. Manfra, “Aharonov–Bohm interference of fractional quantum Hall edge modes,” *Nat. Phys.* **15**, 563 (2019).
- [13] C. D eprez *et al.*, “A tunable Fabry–P erot quantum Hall interferometer in graphene,” *Nature Nanotechnology* **16**, 555 (2021).
- [14] Y. Ronen *et al.*, “Aharonov–Bohm effect in graphene-based Fabry–P erot quantum Hall interferometers,” *Nature Nanotechnology* **16**, 563 (2021).
- [15] M. Peshkin and H. J. Lipkin, “Topology, locality, and Aharonov-Bohm effect with neutrons,” *Phys. Rev. Lett.* **74**, 2847 (1995).
- [16] E. Cohen, H. Larocque, F. Bouchard, F. Nejdastari, Y. Gefen, and E. Karimi, “Geometric phase from Aharonov–Bohm to Pancharatnam–Berry and beyond,” *Nat. Rev. Phys.* **1**, 437 (2019).
- [17] L. E. Ballentine, *Quantum mechanics: A modern development* (World Scientific, Singapore, 2000).
- [18] B. H. Bransden and C. J. Joachain, *Quantum mechanics*, 2nd ed. (Pearson, Harlow, 2000).
- [19] K. Gottfried and T. M. Yan, *Quantum mechanics: Fundamentals*, 2nd ed. (Springer, New York, 2003).
- [20] P. L. Saldanha, “Electrodynamic Aharonov-Bohm effect,” *Phys. Rev. A* **108**, 062218 (2023).
- [21] D. Singleton and E. C. Vagenas, “The covariant, time-dependent Aharonov–Bohm effect,” *Phys. Lett. B* **723**, 241 (2013).
- [22] E. Santos and I. Gonzalo, “Microscopic theory of the Aharonov-Bohm effect,” *EPL* **45**, 418 (1999).
- [23] C. Marletto and V. Vedral, “Aharonov-Bohm phase is locally generated like all other quantum phases,” *Phys. Rev. Lett.* **125**, 040401 (2020).
- [24] P. L. Saldanha, “Local description of the Aharonov–Bohm effect with a quantum electromagnetic field,” *Found. Phys.* **51**, 6 (2021).
- [25] P. L. Saldanha, “Aharonov-Casher and shielded Aharonov-Bohm effects with a quantum electromagnetic field,” *Phys. Rev. A* **104**, 032219 (2021).
- [26] P. L. Saldanha, “Gauge invariance of the Aharonov-Bohm effect in a quantum electrodynamics framework,” *Phys. Rev. A* **109**, 062205 (2024).
- [27] H. Batelaan and A. Tonomura, “The Aharonov–Bohm effects: Variations on a subtle theme,” *Physics Today* **62**, 38 (2009).